ELSEVIER

Fluid Phase Equilibria 174 (2000) 93–113

FLUID PHASE EQUILIBRIA

www.elsevier.nl/locate/fluid

Simplified crossover SAFT equation of state for pure fluids and fluid mixtures

S.B. Kiselev*, J.F. Ely

Department of Chemical Engineering and Petroleum Refining, Colorado School of Mines, Golden, CO 80401-1887, USA

Abstract

A simplified modification of the crossover statistical associating fluid theory (SAFT) EOS is used to describe thermodynamic properties of pure fluids and binary mixtures over a wide range of parameters of state including the nearest vicinity of the critical point. For pure fluids, the simplified crossover (SCR) SAFT model contains only three adjustable parameters but allows an accurate prediction of the critical parameters of pure fluids and yields a better representation of the thermodynamic properties of pure fluids than the original SAFT equation of state. For binary mixtures, simple mixing rules with only one adjustable parameter are used. A comparison is made with experimental data for pure refrigerants R12, R22, R32, R125, R134a, R143a, and mixtures R22+R12, R32+R134a and R125 + R32 in the one- and two-phase regions. The SCR SAFT EOS reproduces the saturated pressure data with an average absolute deviation (AAD) of about 1.1% and the saturated liquid densities with an AAD of about 0.9%. In the one-phase region, the SCR SAFT equation represents the experimental values of pressure with an AAD of about 2.2% in the range of temperatures and density bounded by $T \geq T_c$ and $\rho \leq 2\rho_c$.

Keywords: Critical state; Crossover theory; Equation of state; Hydrofluorocarbons; Mixtures; Thermodynamic properties; Vapor–liquid equilibria

1. Introduction

It is well known that all analytical equations of state fail to reproduce the non-analytical, singular behavior of fluids in the critical region caused by long-scale fluctuations in density. The long-range fluctuations in the density, which involve a huge number of molecules, cause the thermodynamic surface of fluids to exhibit a singularity at the critical point. This asymptotic singular behavior of the thermodynamic properties can be described in terms of scaling laws with universal critical exponents and universal scaling functions [1,2].

Attempts to develop a crossover equation of state which incorporates the scaling laws asymptotically close to the critical point and is transformed into the original classical-analytical EOS far from the critical

* Corresponding author. Tel.: +1-303-273-3190; fax: +1-303-273-3730.
E-mail address: skiselev@mines.edu (S.B. Kiselev).

0378-3812/00/$20.00
PII: S0378-3812(00)00420-9

point have been made by many authors [3–16]. A most general procedure for transforming any classical equation of state into the crossover form was proposed recently by Kiselev [17]. This procedure has a theoretical foundation in the renormalization-group (RG) theory and has been successfully applied to the cubic Patel–Teja (PT) EOS [17,18] and to the statistical associating fluid theory (SAFT) EOS [19].

As was shown by Kiselev and coworkers [17–19], the incorporation of the universal crossover functions into a simple classical EOS not only yields a better description of the *PVT* and vapor–liquid equilibrium (VLE) properties in the critical region, but also improves the representation of the thermodynamic surface of dense fluids in general. As input, the crossover cubic and SAFT EOS developed by Kiselev and coworkers [17–19] requires the original classical EOS parameters, the critical temperature and density and at least three additional system-dependent parameters more then original classical EOS.

Recently, Jiang and Prausnitz [20] presented a related paper using an equation of state for chain fluids (EOSCF) and a global RG method developed by White et al. [8–10]. Their crossover model contains fewer the adjustable parameters than the crossover SAFT EOS [17,18], but the EOSCF + RG equations can be solved only numerically and require an additional spline function for a representation of the thermodynamic surface of real fluids.

The thermodynamic surface of binary mixtures in the critical region differs substantially from that observed in pure fluids. In the critical region a mixture displays a regime of pure-fluid-like behavior at fixed field variable (chemical potential μ) rather than at fixed composition x [21–24]. As a consequence, all thermodynamic properties calculated at fixed composition are renormalized in the critical region of a binary mixture [2,24,25]. There are few crossover models of mixtures formulated in terms of the chemical potential that incorporate scaling laws in the critical region. Namely, the six-term crossover model developed by Sengers and coworkers [26,27], the crossover Leung–Griffiths model developed by Belyakov et al. [28], and the more extensive parametric crossover model developed by Kiselev [29]. In Kiselev's approach [29,30], all parameters of the theory are expressed as functions of the excess critical compressibility factor of the mixture. Therefore, if the critical locus of the mixture is known, all other thermodynamic properties can be predicted [29–33]. So far, all of these crossover equations were developed for Type I binary mixtures only and they do not reproduce the ideal gas equation of state in the limit of low densities.

In this paper, we continue our study of the crossover SAFT EOS initiated in our previous work [19]. We present a new, simplified crossover SAFT EOS which contains the same number of the adjustable parameters as original SAFT EOS but yields much better representation of the thermodynamic surface of pure fluids than original SAFT EOS. In order to extend this EOS to mixtures we formulate the mixing rules in terms of compositions and develop the simplified crossover SAFT EOS for fluid mixtures.

2. Crossover SAFT model

In order to obtain the crossover formulation of the SAFT EOS one needs to start from the classical formulation of the Helmholtz free energy density. The original SAFT EOS is given in terms of the residual Helmholtz free energy per mole [34].

$$a(T, v) = a^{\text{res}}(T, v) + a^{\text{ideal}}(T, v) \tag{1}$$

where $a(T, v)$ is the total Helmholtz free energy, $a^{\text{res}}(T, v)$ is the residual Helmholtz free energy, and $a^{\text{ideal}}(T, v) = -RT\ln(v) + a_0(T)$ is the ideal gas Helmholtz free energy per mole at the same temperature

T and molar volume $v = V/N$. A general method for transforming any classical equation of state into a crossover equation was described in detail by Kiselev [17]; therefore, we will not reproduce it here. In the present work, we will use the crossover SAFT EOS obtained with Kiselev's method given in our previous publication [19].

The final expression for the dimensionless crossover Helmholtz free energy $\bar{A}(T, v) = a(T, v)/RT$ for the SAFT equation of state can be written in the form [19]

$$\bar{A}(T, v) = \Delta\bar{A}(\bar{\tau}, \Delta\bar{\eta}) - \Delta v\bar{P}_0(T) + \bar{A}_0^{\text{res}}(T) + \bar{A}_0(T) - \mathcal{K}(\tau^2) \tag{2}$$

where $\Delta v = v/v_{0c} - 1$ is the classical order parameter, $\tau = T/T_c - 1$ is the dimensionless deviation of the temperature from the critical temperature T_c, and $\Delta\eta = v/v_c - 1$ is the dimensionless deviation of the molar volume v from the critical volume v_c, and $\bar{\tau}$ and $\Delta\bar{\eta}$ are their renormalized values to be specified below. The critical part of the dimensionless Helmholtz free energy is

$$\Delta\bar{A}(\bar{\tau}, \Delta\bar{\eta}) = \bar{A}^{\text{res}}(\bar{\tau}, \Delta\bar{\eta}) - \bar{A}^{\text{res}}(\bar{\tau}, 0) - \ln(\Delta\bar{\eta} + 1) + \Delta\bar{\eta}\bar{P}_0(\bar{\tau}) \tag{3}$$

where the dimensionless residual part of the Helmholtz free energy $\bar{A}^{\text{res}} = a^{\text{res}}/RT$ is given by

$$\bar{A}^{\text{res}}(\bar{\tau}, \Delta\bar{\eta}) = m\left[\frac{4\bar{\eta} - 3\bar{\eta}^2}{(1-\bar{\eta})^2} + \sum_i\sum_j D_{ij}\left(\frac{u}{kT_{0c}(\bar{\tau}+1)}\right)^i\left(\frac{\bar{\eta}}{\eta_0}\right)^j\right] + (1-m)\ln g^{\text{hs}}(\bar{\eta}) + \bar{A}^{\text{assoc}}(\bar{\tau}, \Delta\bar{\eta}) \tag{4}$$

where D_{ij} are universal constants [35],

$$g^{\text{hs}}(\bar{\eta}) = \frac{2 - \bar{\eta}}{2(1-\bar{\eta})^3} \tag{5}$$

is a hard sphere radial distribution function at contact, $\bar{\eta}=\eta_{0c}/(\Delta\bar{\eta} + 1)$ is the renormalized reduced density, $\eta_{0c} = \eta_0 m v^0/v_{0c}$ is the reduced critical density, $\eta_0 = 0.74048$. In Eqs. (1)–(4) R is the universal gas constant, k the Boltzmann constant, and the parameters v^0 and u are given by

$$v^0 = v^{00}\left[1 - C\exp\left(\frac{-3u^0}{kT_{0c}(\bar{\tau}+1)}\right)\right]^3 \tag{6}$$

$$u = u^0\left(1 + \frac{e}{kT_{0c}(\bar{\tau}+1)}\right) \tag{7}$$

where $C = 0.12$, $e/k = 10$, and v^{00} and u^0 are system-dependent parameters. The last term in (4) corresponds the Helmholtz free energy change due to association [19]. An explicit expression for this term and the crossover SAFT EOS for self-associated fluids are discussed in [19,36]. Since self-associated fluids are not considered in this work, we set $\bar{A}^{\text{assoc}} = 0$.

In Eqs. (2)–(7), the parameters T_{0c} and v_{0c} are the classical critical parameters found from the original SAFT EOS through the conditions

$$P_{0c} = -\left(\frac{\partial a}{\partial v}\right)_{T_{0c}}, \qquad \left(\frac{\partial^2 a}{\partial v^2}\right)_{T_{0c}} = 0, \qquad \left(\frac{\partial^3 a}{\partial v^3}\right)_{T_{0c}} = 0 \tag{8}$$

These equations for the SAFT EOS can be solved only numerically. In general, the critical parameters in the original SAFT EOS T_{0c}, v_{0c}, and P_{0c} are the complicated functions of the parameters m, v^{00}, and u^0, do not coincide with the real (experimental) critical parameters T_c, v_c, and P_c.

The renormalized pressure $\bar{P}_0(\bar{\tau})$ is given by [19]

$$\bar{P}_0(\bar{\tau}) = m\left[\frac{4\eta_{0c}-2\eta_{0c}^2}{(1-\eta_{0c})^3} + \sum_i\sum_j jD_{ij}\left(\frac{u}{kT_{0c}(\bar{\tau}+1)}\right)^i\left(\frac{\eta_{0c}}{\eta_0}\right)^j\right] + (1-m)\frac{5\eta_{0c}-2\eta_{0c}^2}{(1-\eta_{0c})(2-\eta_{0c})} \tag{9}$$

and the temperature-dependent functions $\bar{A}_0^{res}(T)$ and $\bar{P}_0(T)$ in Eq. (2) are given by

$$\bar{A}_0^{res}(T) = m\left[\frac{4\eta_{0c}-3\eta_{0c}^2}{(1-\eta_{0c})^2} + \sum_i\sum_j D_{ij}\left(\frac{u}{kT}\right)^i\left(\frac{\eta_{0c}}{\eta_0}\right)^j\right] + (1-m)\ln g^{hs(\eta_{0c})} \tag{10}$$

$$\bar{P}_0(T) = m\left[\frac{4\eta_{0c}-2\eta_{0c}^2}{(1-\eta_{0c})^3} + \sum_i\sum_j jD_{ij}\left(\frac{u}{kT}\right)^i\left(\frac{\eta_{0c}}{\eta_0}\right)^j\right] + (1-m)\frac{5\eta_{0c}-2\eta_{0c}^2}{(1-\eta_{0c})(2-\eta_{0c})} \tag{11}$$

where the hard sphere distribution function g^{hs} is given by the Eq. (5) with $\bar{\eta} = \eta_{0c}$, and parameters v^0 and u are given by Eqs. (6) and (7). Eqs. (9) and (11) have a similar form with the principal difference between them being that $\bar{P}_0$ in Eq. (11) is a function only of the temperature T, while $\bar{P}_0$ as given by Eq. (9) is a function of the renormalized temperature $\bar{\tau}$, which depends on both variables, T and v.

The renormalized temperature $\bar{\tau}$ and order parameter $\Delta\bar{\eta}$ in Eqs. (2)–(9) are related to the real dimensionless temperature τ and the real order parameter $\Delta\eta$ through

$$\bar{\tau} = \tau Y^{-\alpha/2\Delta_1} + (1+\tau)\Delta\tau_c Y^{2(2-\alpha)/3\Delta_1} \tag{12}$$

$$\Delta\bar{\eta} = \Delta\eta Y^{(\gamma-2\beta)/4\Delta_1} + (1+\Delta\eta)\Delta\eta_c Y^{(2-\alpha)/2\Delta_1} \tag{13}$$

where the factors $\Delta\tau_c = \Delta T_c/T_{0c} = (T_c - T_{0c})/T_{0c}$ and $\Delta\eta_c = \Delta v_c/v_{0c} = (v_c - v_{0c})/v_{0c}$ are the dimensionless shifts of the real critical temperature T_c and the real critical volume v_c from the classical values, T_{0c} and v_{0c}, defined by Eqs. (8) and Eqs. (12) and (13) with $\Delta\tau_c \neq 0$ and $\Delta\eta_c \neq 0$ automatically provide the critical conditions

$$\left(\frac{\partial^2\bar{A}}{\partial v^2}\right)_{T_c(v=v_c)} = 0, \qquad \left(\frac{\partial^3\bar{A}}{\partial v^3}\right)_{T_c(v=v_c)} = 0 \tag{14}$$

(compare with the critical conditions for the classical SAFT EOS given by Eq. (8)). Thus, using the non-zero critical shifts in Eqs. (12) and (13) one can set for the crossover SAFT EOS the real experimental values of the critical temperature T_c and volume v_c, while the critical pressure

$$P_c = -RT\left(\frac{\partial\bar{A}}{\partial v}\right)_{T_c(v=v_c)} \tag{15}$$

for the crossover SAFT EOS remains a complicated function of the parameters m, v^{00}, u^0, T_c, and v_c.The kernel term in Eq. (2) gives rise to a heat capacity divergence along the critical isochore and can be written as

$$\mathcal{K}(\tau^2) = \tfrac{1}{2}a_{20}\tau^2(Y^{-\alpha/\Delta_1} - 1) + \tfrac{1}{2}a_{21}\tau^2(Y^{-(\alpha-\Delta_1)/\Delta_1} - 1) \tag{16}$$

where the first term corresponds to the asymptotic limit and the second term to the first Wegner correction for the isochoric specific heat [37]. In Eqs. (12)–(16), $\gamma = 1.24,\ \beta = 0.325,\ \alpha = 2-\gamma-2\beta = 0.110$, and $\Delta_1 = 0.51$ are the universal non-classical critical exponents. The crossover function Y in Eqs. (12)–(16) is represented in the parametric form [18]

$$Y(q) = \left(\frac{q}{1+q}\right)^{2\Delta_1} \tag{17}$$

which corresponds to the theoretical crossover function obtained by Belyakov et al. [28] in the first order of an ϵ-expansion.

In Eq. (17) the parametric variable $q^2 = r/Gi$, where r has a meaning of a dimensionless measure of the distance from the critical point, and Gi is the Ginzburg number of a fluid of interest [17,38,39]. In our previous work [19], we found the variable r from a solution of the parametric linear model (LM) EOS. The LM EOS has a theoretical foundation in the renormalization-group theory and was confirmed in the second order of an ϵ-expansion [40], but it cannot be extended into the metastable region or represent analytically connected van der Waals loops. Therefore, in the present work, we find the variable r from a solution of the parametric sine model developed recently by Fisher and coworkers [41]:

$$\tau = r\left(1 - 2b^2\frac{[1-\cos(p\theta)]}{p^2}\right), \qquad \Delta\eta = m_0 r^\beta \frac{\sin(p\theta)}{p} \tag{18}$$

where (r, θ) are the parametric variables, m_0 an adjustable parameter, while b^2 and p^2 are the universal sine-model parameters. Unlike the linear model employed earlier by Kiselev and coworkers [17–19], the sine model with the parameter $p_-^2 < p^2 < p_+^2$, where

$$p_\pm^2 = 2b^2[1 \pm 2\sqrt{(1-\beta)}] \tag{19}$$

Table 1
Constants in Eqs. (23)–(26) for the SCR SAFT EOS

Coefficients	
δ_τ	3.4×10^{-2}
$v_1^{(0)}$	-4.9×10^{-2}
$d_1^{(0)}$	0.166
δ_ρ	5.4
$v_1^{(1)}$	5.0×10^{-3}
$d_1^{(1)}$	5.5

the parameters d_1^0 and d_1^1 in Eq. (26), are not sensitive to the choice of fluid. Therefore, in the simplified crossover (SCR) SAFT EOS, all these parameters were considered constant. The values of all universal parameters for the SCR SAFT EOS are given in Table 1.

In this study, we have applied the SCR SAFT EOS for the description of the experimental data of refrigerants R12, R22, R32, R125, R134a, and R145a in the one- and two-phase regions. Similar to the crossover SAFT EOS for *n*-alkanes [19], the inverse Ginzburg number $g = 1/Gi$ for hydrofluorocarbons was represented as linear function of the molecular weight:

$$g = g^{(0)} + g^{(1)} M_w \tag{27}$$

where the parameters $g^{(0)} = 6.6345$ and $g^{(1)} = 0.0945$ were found from a fit of the SCR SAFT EOS to the VLE data for R32 and R125. After the determination of the parameter g, only three adjustable parameters m, v^{00}, and u^0 in the SCR SAFT EOS were left. For all refrigerants, we found these parameters from a fit of the SCR SAFT EOS only to saturated pressure and liquid density data. The values of all system-dependent parameters, together with calculated and experimental values of the critical parameters for R12, R22, R32, R125, R134a, and R145a, are given in Table 2. Good agreement between calculated and experimental values of critical parameters is observed. The maximum deviation of the calculated values from the experimental ones does not exceed 0.6 K for T_c (or about 0.17%), 0.25 mol l^{-1} (or about 4%) for ρ_c, and 0.1 MPa (or about 2%) for P_c. A comparison of the saturated pressure data with the values calculated with SCR SAFT EOS is shown in Fig. 1. The calculated and experimental values of saturated liquid densities are shown in Fig. 2. The percentage deviations of experimental saturated pressures and liquid densities from the values calculated with the simplified crossover SAFT equation of state are given in Fig. 3. The SCR SAFT EOS describes the saturated pressures and liquid densities for all refrigerants with an average absolute deviation (AAD) of about 1%.

Unlike our previous crossover SAFT EOS based on the LM EOS for the parametric variable q [19], the SCR SAFT EOS not only gives an accurate representation of the thermodynamic properties of pure fluids in the two-phase region but also is capable of representing the analytically connected van der Waals loops in the metastable region. The van der Waals loops calculated for refrigerant R32 with the SCR SAFT EOS are shown in Fig. 4.

Since in the optimization of the model no experimental data in the one-phase region were used, it is interesting to test the predictions of the model in the one-phase region. A comparison of the calculated liquid density with experimental data for R134a is shown in Fig. 5. The maximum deviation of the experimental densities from the calculated ones for all points presented in Fig. 6 does not exceed

Table 2
System-dependent constants for the simplified crossover SAFT EOS

Parameter	R12	R22	R32	R125	R134a	R143a
v^{00} (mL.mol^{-1})	9.1736	6.4522	4.0768	5.7531	4.9959	6.1525
m	4.2972	4.7746	5.6816	6.0515	6.5899	5.6319
u^0/k (K)	153.17	140.02	124.18	116.85	125.18	122.70
M_w	120.91	86.469	52.024	120.00	102.03	84.044
ω	0.177	0.221	0.277	0.303	0.327	0.261
Critical parameters[a]						
T_c^{calc} (K)	385.40	368.94	351.50	339.67	374.72	346.47
T_c^{exp} (K)	385.01	369.32	351.35	339.33	374.27	345.88
ρ_c^{calc} (mol.L^{-1})	4.7692	6.2044	8.3855	4.8398	5.0856	5.2505
ρ_c^{exp} (mol.L^{-1})	4.6974	5.9559	8.2008	4.7600	5.1390	5.1282
P_c^{calc} (MPa)	4.0991	4.8245	5.7003	3.5961	4.0457	3.7812
P_c^{exp} (MPa)	4.1290	4.9210	5.7950	3.6290	4.0650	3.7640
Average absolute deviation (AAD%)[b]						
P_{sat}	0.87	1.27	1.10	1.14	1.13	1.34
ρ_{sat}^L	0.95	0.71	1.95	0.53	0.53	0.95
PVT	2.88	1.99	2.09	2.24	1.84	2.48

[a] Superscripts "calc" and "exp" correspond to the calculated and experimental values, respectively. The experimental critical parameters were taken from [31] for R12 and R22, from [33] for R32, R125 and R134a, and from [55] for R143a.

[b] AAD calculated in the temperature region $0.7T_c \leq T \leq T_c$ for P_{sat}, at $0.5T_c \leq T \leq T_c$ for ρ_{sat}^L, and in the one-phase region at $T \geq T_c$ and $\rho \leq 2\rho_c$ for PVT data.

0.6 mol l^{-1}, or about 4%. These deviations are mostly observed at low temperatures viz. $T \leq 0.7T_c$, or $u/kT \geq 0.6$. Since for simple non-associating fluids the SAFT EOS is simply a combination of the repulsive hard-sphere contribution and the dispersion term which is represented in the power series of u/kT [34], it is not surprising that at lower temperatures where $u/kT \approx 1$ the crossover SAFT EOS gives

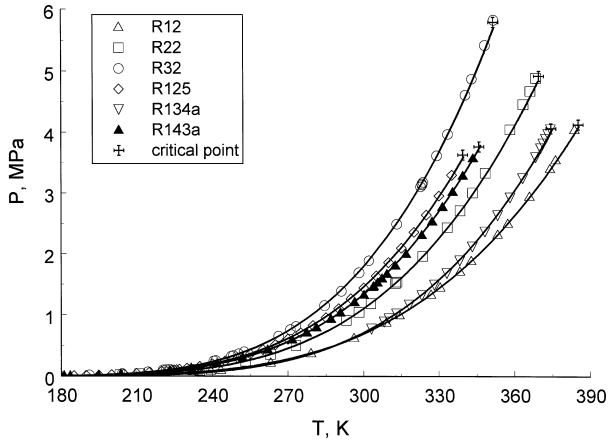

Fig. 1. Saturated pressure data for R12 [56–58], R22 [59,60], R32 [61], R125 [62], R134a [63], and R143a [64] (symbols) with predictions of the simplified crossover SAFT equation of state (lines).

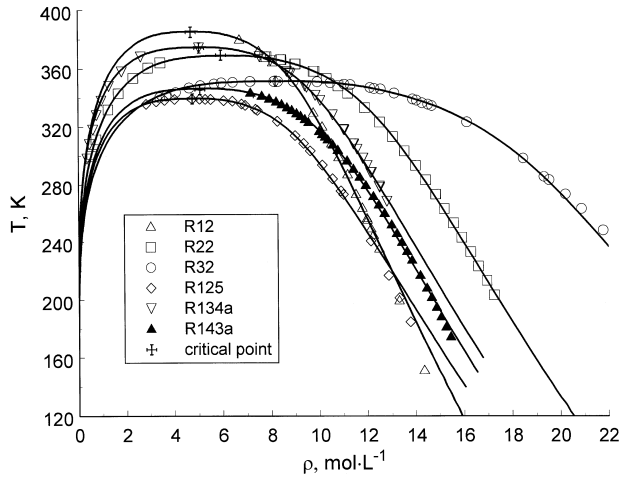

Fig. 2. Saturated density data for R12 [65], R22 [66], R32 [61], R125 [62,67,68], R134a [69], and R143a [64] (symbols) with predictions of the simplified crossover SAFT equation of state (lines).

worse results than in the high-temperature region, at $u/kT \ll 1$. In order to improve the representation of experimental data with the crossover SAFT EOS in the region $u/kT \approx 1$, the original SAFT EOS should be improved first. One way of doing this is to include into the original SAFT EOS the additional dipolar and quadrupolar contributions as was done, for example, in the BACKONE equations [45]. However, one should admit that even in the present form, the SCR SAFT EOS yields a major improvement in

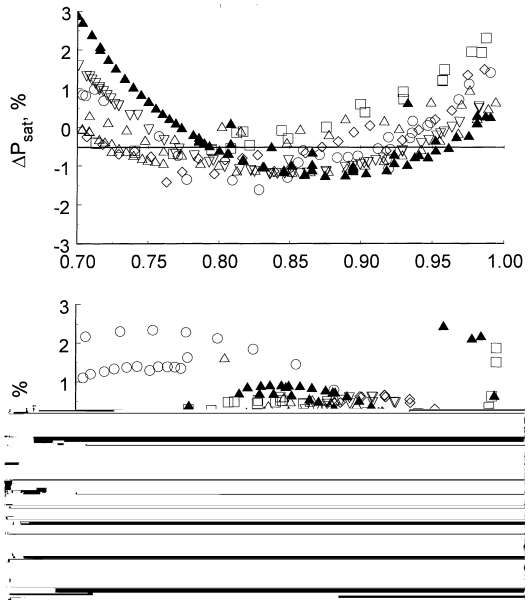

Fig. 3. Percentage deviations of experimental saturated pressures (top) and saturated liquid densities (bottom) for pure refrigerants from the values calculated with the simplified crossover SAFT equation of state. Legend as in Figs. 1 and 2.

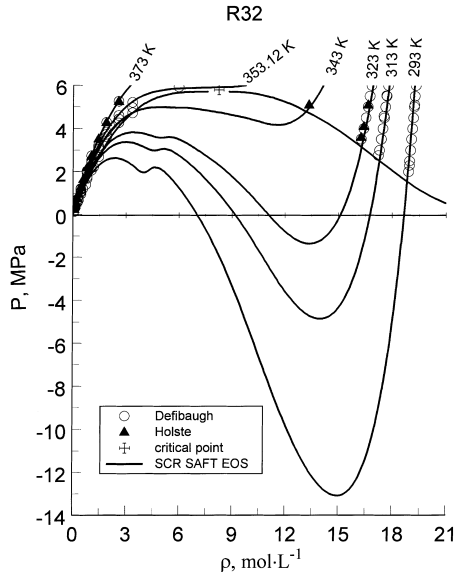

Fig. 4. The van der Waals loops for refrigerant R32 calculated with the simplified crossover SAFT equation of state. The symbols represent experimental data obtained by Defibaugh et al. [70] and by Holste et al. [71].

the description of the *PVT* surface of pure refrigerants in the one- and two-phase regions. In Fig. 6, we show the calculated pressures in comparison with experimental data for R32. The dashed curves in Fig. 6 correspond to the values calculated with crossover Patel–Teja (CR PT) EOS [17]. As one can see, the SCR SAFT EOS yields much better representation of the high-density *PVT* data than CR PT EOS. The values of AAD for pressure in the one- and two-phase region for all refrigerants are presented in Table 2.

We need to note that the values of AAD presented in Table 2 for the one-phase region are not a result of a fit of the SCR SAFT EOS to experimental data in the one-phase region, but a pure prediction of the model

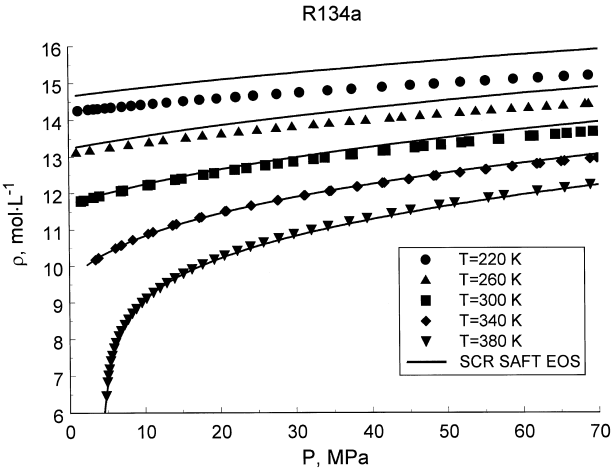

Fig. 5. Liquid density data [72] for R134a (symbols) with predictions of the simplified crossover SAFT equation of state (lines).

Fig. 6. $P\rho T$ data [61,70,71] for R32 (symbols) with predictions of the simplified crossover SAFT equation of state (solid lines) and with the crossover cubic EOS [17] (dashed lines).

with the parameters obtained for the two-phase region. We are not aware of any other three-parameter model with the same power of predictability. Recently, Fermeglia et al. [46] presented a comparison with

while for the energetic parameter $u^0(x)$, we adopt the van der Waals mixing rule:

$$u^0(x) = \sum_i \sum_j x_i x_j u^0_{ij} \tag{29}$$

associated with the quadratic equation

$$u^0_{ij} = \sqrt{u^0_i u^0_j}(1 - k_{ij}), \quad k_{ij} = k_{ji}, k_{ii} = k_{jj} = 0 \tag{30}$$

where k_{ij} is a binary interaction parameter. With these mixing rules, the critical parameters which appear in Eqs. (2)–(11) are not anymore the real critical parameters of a mixture which can be found from the conditions

$$\left(\frac{\partial \mu}{\partial x}\right)_{P_c, T_c(v=v_c)} = 0, \qquad \left(\frac{\partial^2 \mu}{\partial x^2}\right)_{P_c, T_c(v=v_c)} = 0 \tag{31}$$

but the pseudo-critical parameters which are determined by Eqs. (14). This is a major simplification of the model. The mixing rules as given by Eqs. (28)–(30) are simpler than those derived by Huang and Radosz [47,48] for the original SAFT EOS then the more rigorous critical region field-variable mixing rules adopted in [26–30]. However, as we show below, using these simple mixing rules, the SCR SAFT EOS yields a satisfactory representation of the thermodynamic properties of mixtures of hydrofluorocarbons in a large range of temperatures and densities.

We have chosen the refrigerant mixtures R22 + R12, R32 + R134a, and R125 + R32 for comparison with the model. The interaction parameters were $k_{12} = 0.04$ for R22+R12, $k_{12} = 0.005$ for R32+R134a, and $k_{12} = 0.02$ for the R125+R32 mixture. These values were obtained from a fit of the SCR SAFT EOS to the experimental *PVTx* data in the one-phase region obtained by Takaishi et al. [49] for the R22 + R12 mixture and by Magee and Haynes [50] for R32 + R134a and R125 + R32 mixtures. A comparison of the calculated values of pressure along isochores with experimental data of Takaishi et al. [49] is presented in

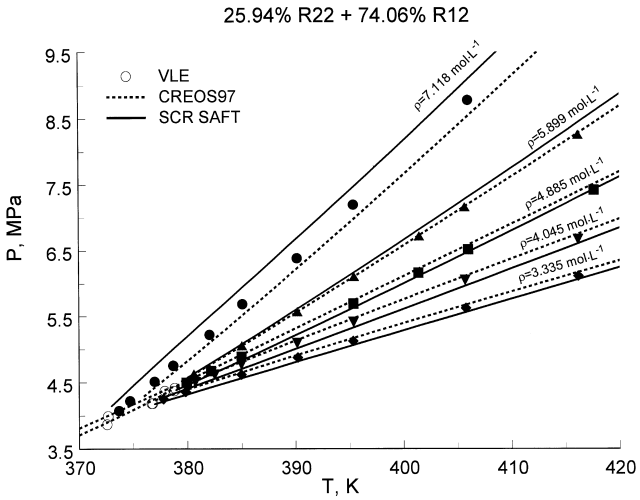

Fig. 7. *PVT* data for the R22 + R12 mixture obtained by Takaishi et al. [49] with predictions of the computer program CREOS97 (dashed curves) and the simplified crossover SAFT equation of state (solid curves).

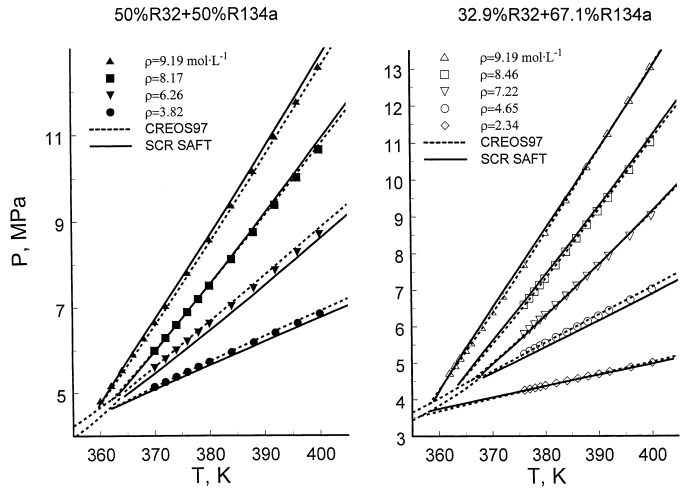

Fig. 8. *PVT* data for R32 + R134a mixtures obtained by Magee and Haynes [50] (symbols) with predictions of the computer program CREOS97 (dashed curves) and the simplified crossover SAFT equation of state (solid curves).

Fig. 7. Figs. 8 and 9 compare the values obtained from our model with the *PVTx* data of Magee and Haynes [50]. The dashed curves in all figures represent the values calculated with the parametric crossover model (computer program CREOS97) obtained in [31] for the R22 + R12 mixture and in [33] for R32 + R134a and R125 + R32 mixtures (Fig. 10). The SCR SAFT model shows good agreement for all mixtures. The maximum deviation of the calculated values of pressure from the experimental ones does not exceed 2%.

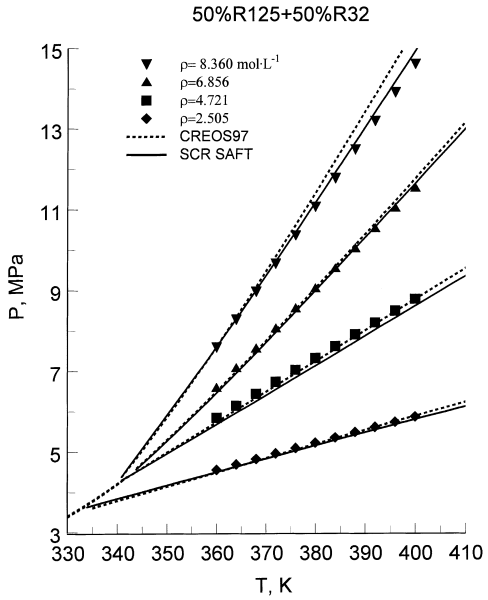

Fig. 9. *PVT* data for R125 + R32 mixtures obtained by Magee and Haynes [50] (symbols) with predictions of the computer program CREOS97 (dashed curves) and the simplified crossover SAFT equation of state (solid curves).

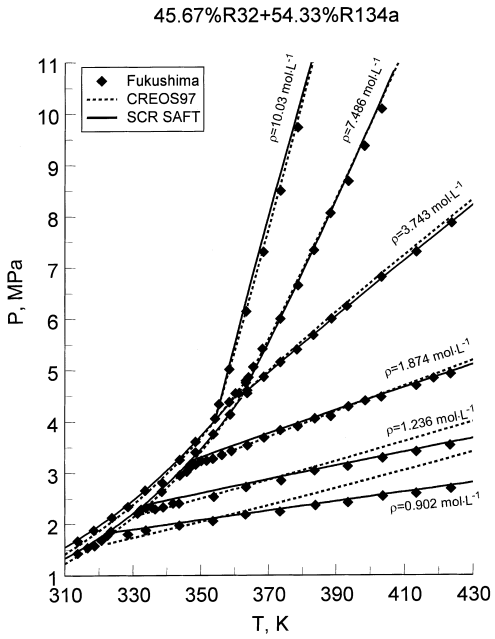

Fig. 10. *PVT* data for R32 + R134a mixtures obtained by Fukushima and co-workers [51] (symbols) with predictions of the computer program CREOS97 (dashed curves) and the simplified crossover SAFT equation of state (solid curves).

Only for the R22 + R12 mixture along the isochore $\rho = 7.118\,\mathrm{mol.L^{-1}}$, systematic deviations up to 4% are observed.

In Fig. 9, we compare the predictions of the model for *PVTx* properties for a 45.67 mol% R32 + 54.33 mol% R134a system with the experimental data of Fukushima et al. [51]. The data are over a wide range of temperatures from 314 to 424 K and at pressures from 1.5 to 10.1 MPa, and densities over the range $\rho = 0.902$–$10.033\,\mathrm{mol\,l^{-1}}$. Since these data were not used for the optimization of the model, this is a good test of the predictability of the model. The SCR SAFT EOS shows good agreement with the data, while the parametric crossover model gives systematic deviation from the experimental data at isochores $\rho = 0.902$ and $1.236\,\mathrm{mol\,l^{-1}}$. This deviation is a direct consequence of the fact that the parametric crossover model fails to reproduce the ideal gas limit.

Even though the parameters for k_{ij} were found using one-phase data, the SCR SAFT EOS can be extrapolated into the two-phase region. Figs. 11–14 show the VLE coexistence curves for R22 + R12, R32 + R134a, and R125 + R32 mixtures in the critical region and below. The model agrees very well with the data up to temperatures $T = 0.99T_c(x)$. For calculations of the VLE properties of the mixtures, we used an iterative algorithm developed by Lemmon [52]. As was also pointed out in [18], this algorithm does not converge very close to the critical point of a mixture, at $|\tau(x)| \leq 10^{-2}$, and alternative algorithms should be used. For comparison, we also have shown the predictions from the parametric crossover model CREOS97 [33] and NIST REFPROP [53]. As one can see, far from the critical point, all models give practically identical results which are in good agreement with experimental data. However, as the critical point approaches the NIST REFPROP, predictions become less accurate and exhibit systematic deviations from experimental data, while the SCR SAFT EOS yields a reasonably good description of experimental

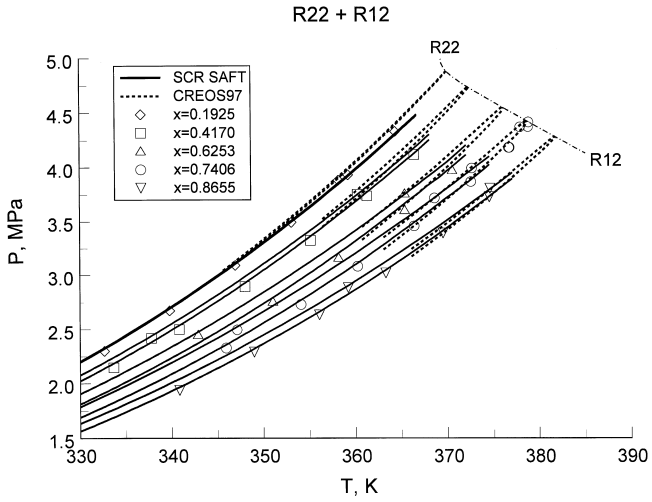

Fig. 11. Dew-bubble curves for R22 + R12 mixtures. The symbols indicate experimental data obtained by obtained by Takaishi et al. [49], and the curves represent predictions from the computer program CREOS97 (dashed curves) and the simplified crossover SAFT equation of state (solid curves).

data up to $T = 0.99T_c(x)$. Fig. 15 shows the experimental VLE data for R125 + R32 mixtures obtained by Higashi [54] at four isotherms far from the critical point with the predictions of the SCR SAFT EOS, the parametric crossover model CREOS97 [33], and NIST REFPROP [53]. Quantitatively, all models give similar predictions which are in good agreement with experimental data; however, qualitatively,

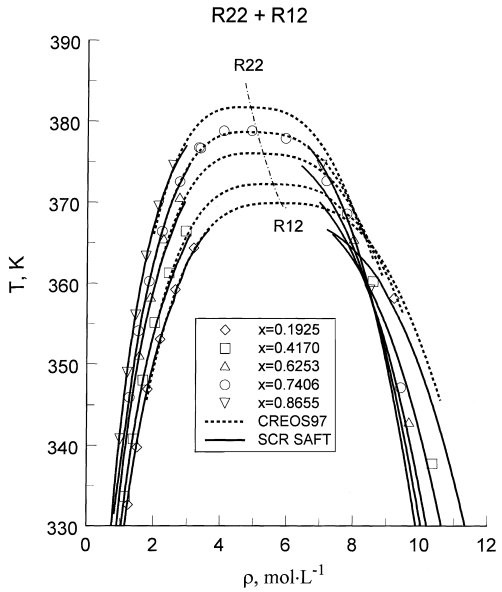

Fig. 12. VLE data for R22 + R12 mixtures obtained by Takaishi et al. [49] (symbols) with predictions of the computer program CREOS97 (dashed curves) and the simplified crossover SAFT equation of state (solid curves).

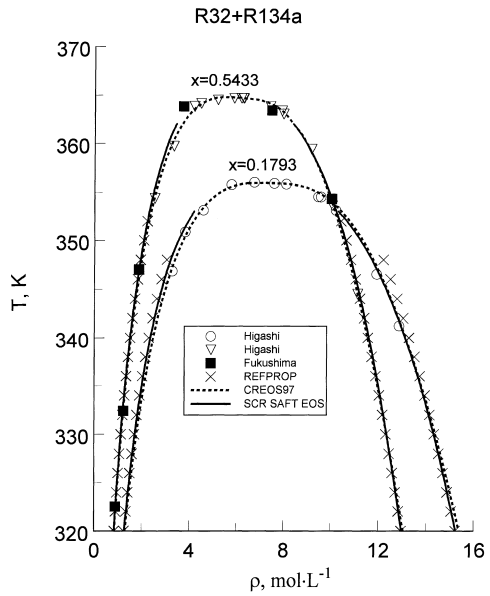

Fig. 13. VLE data for R32 + R134a mixtures of Higashi [73] and of Fukushima [74] at two concentrations of R134a and predictions from the computer program NIST REFPROP [53], the computer program CREOS97 (dashed curves), and of the simplified crossover SAFT model (solid curves).

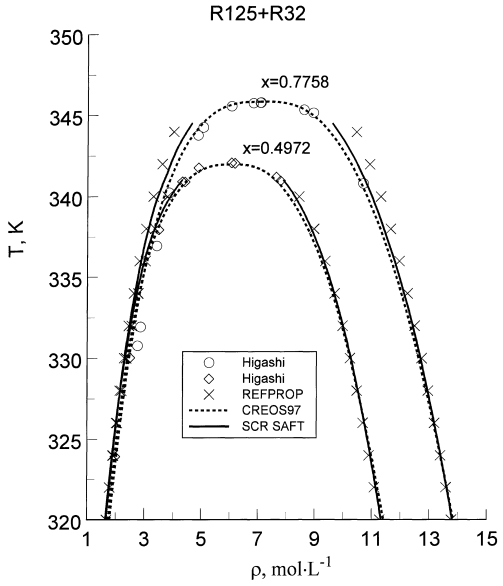

Fig. 14. VLE data for R125 + R32 mixtures of Higashi [54] at two concentrations of R32 and predictions from the computer program NIST REFPROP [53], the computer program CREOS97 (dashed curves), and of the simplified crossover SAFT model (solid curves).

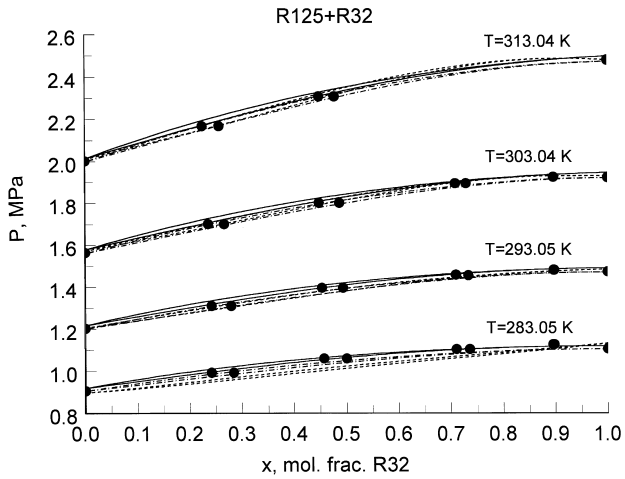

Fig. 15. The pressure–composition diagram for R125 + R32 mixtures. The symbols indicate experimental data obtained by Higashi [54] at four temperatures, and the curves represent predictions from the computer program CREOS97 (dashed curves), the computer program NIST REFPROP [53] (dashed–dotted curves), and of the simplified crossover SAFT model (solid curves).

the results are different. Experimental data obtained by Higashi for R125 + R32 mixtures [54] exhibit the appearance of an azeotrope at approximately 90 mol% R32 at temperatures less than $T = 303\,\mathrm{K}$. The SCR SAFT model predicts the appearance of an azeotrope at $T \leq 283\,\mathrm{K}$, the computer program CREOS97 predicts an azeotrope at temperatures $T \geq 303\,K$. The newest version of NIST REFPROP [75,76] predicts a very weak azeotrope for R125+R32 mixtures at P=0.1–0.4 MPa at compositions of about 0.9 mole fraction R32. By P=1 MPA, the azeotrope disappears. We cannot say for sure which prediction is correct. In order to answer this question, more experimental information for this mixture is needed.

5. Conclusions

On the basis of the crossover SAFT EOS obtained before [19], we develop a simplified crossover modification of the SAFT equation of state which, similar to the original SAFT EOS, contains only three adjustable parameters but gives an accurate prediction of the critical parameters for pure fluids and yields a much better representation of the *PVT* and VLE properties pure fluids in and beyond the critical region than original SAFT EOS and CR PT EOS [17]. Unlike our previous crossover EOS based on the linear model EOS for the parametric variable q [17,19], the SCR SAFT EOS based on the parametric sine model [41] can be extended into the metastable region and represents analytically connected van der Waals loops. In the present work, we tested the SCR SAFT EOS experimental data again for pure refrigerants in the one- and two-phase regions. Good agreement with experimental *PVT* and VLE data was achieved in the wide rage of the parameters of state including the critical region.

In order to extend the crossover SAFT EOS to mixtures, we formulate the simple mixing rules for the system-dependent parameters of the model in terms of composition. Although with these simplified mixing rules the crossover SAFT EOS does not reproduce some of the known scaling laws in the asymptotic

critical region of mixtures, at dimensionless temperatures $|\tau(x)| \geq 10^{-2}$, it yields an accurate representation of the thermodynamic surface of the mixtures of hydrofluorocarbons in the one- and two-phase regions. To extend the obtained results to other, more complex fluids and their mixtures, the model should be checked with other mixing rules, with a more rigorous theoretical basis.

List of symbols

a	Helmholtz free energy per mole (total, res, assoc, etc.)
a_{2i}	coefficients in the kernel term ($i = 0$ and $i = 1$)
$\bar{A}$	dimensionless Helmholtz free energy (total, res, etc.)
b^2	universal linear-model parameter
C	integration constant in Eq. (6)
d_1	rectilinear diameter amplitude
$d_1^{(j)}$	constants in Eq. (26) ($j = 0, 1$)
D_{ij}	universal constants in Eq. (4)
e/k	constant in Eq. (7) (K)
g^{hs}	hard sphere radial distribution function
Gi	Ginzburg number
$\Delta\eta$	order parameter
k	Boltzmann's constant $\approx 1.3814 \times 10^{-23}$ J/K
k_{ij}	binary interaction parameter
$\mathcal{K}$	kernel term
m	number of segments
m_0	sine-model critical amplitude
M_{w}	molecular weight
N	total number of molecules
p^2	universal sine-model parameter
P	pressure
P_{c}	critical pressure
q	argument of crossover function
r	parametric variable
R	gas constant
T	temperature (K)
T_{c}	critical temperature (K)
ΔT	dimensionless deviation of the temperature from the classical critical temperature
u/k	temperature-dependent dispersion energy of interaction between segments (K)
u^0/k	temperature-independent dispersion energy of interaction between segments (K)
v	molar volume
v_1	system-dependent coefficient in Eq. (21)
$v_1^{(j)}$	coefficients in Eq. (25) ($j = 0, 1$)
v^0	temperature-dependent segment volume
v^{00}	temperature-independent segment volume
Δv	classical order parameter
Δv_{c}	shift of the critical volume

V total volume
x composition of a mixture
Y crossover function

Greek letters
α universal critical exponent
β universal critical exponent
δ_1 universal constant in Eq. (21)
δ_τ constant in Eq. (23)
δ_ρ constant in Eq. (24)
$\Delta\bar{\eta}$ re-scaled order parameter
$\Delta\eta_c$ dimensionless shift of the critical volume
Δ difference
Δ_1 universal critical exponent
γ universal critical exponent
μ chemical potential of a mixture
τ reduced temperature difference
$\Delta\tau_c$ dimensionless shift of the critical temperature
$\bar{\tau}$ re-scaled reduced temperature difference
θ parametric variable
ρ molar density
ρ_c critical density (mol/l)

Superscripts
assoc association
G gas
ideal ideal gas
L liquid
res residual

Subscripts
c critical
sat saturated
0 classical

Acknowledgements

The authors are indebted to M. Fisher for providing us with the manuscript of his paper prior to publication. The research was supported by the US Department of Energy, Office of Basic Energy Sciences, under Grant No. DE-FG03-95ER41568.

References

[1] J.V. Sengers, J.M.H. Levelt Sengers, Annu. Rev. Phys. Chem. 37 (1986) 189.

[2] M.A. Anisimov, S.B. Kiselev, in: A.E. Scheindlin, V.E. Fortov (Eds.), Sov. Tech. Rev. B. Therm. Phys., Vol. 3, Part 2, Harwood, New York, 1992, pp. 1–121.
[3] J.R. Fox, Fluid Phase Equilibria 14 (1983) 45.
[4] A. Parola, L. Reatto, Phys. Rev. A 31 (1985) 3309.
[5] M. Tau, A. Parola, D. Pini, L. Reatto, Phys. Rev. E 52 (1995) 2644.
[6] L. Reatto, A. Parola, J. Phys.: Condens. Matter 8 (1996) 9221.
[7] L. Lue, J.M. Praustitz, AIChE J. 44 (1998) 1455.
[8] J.A. White, Fluid Phase Equilibria 75 (1992) 53.
[9] J.A. White, S. Zhang, J. Chem. Phys. 99 (1993) 2012.
[10] J.A. White, S. Zhang, J. Chem. Phys. 103 (1995) 1922.
[11] J.A. White, J. Chem. Phys. 111 (1999) 9352.
[12] J.A. White, J. Chem. Phys. 112 (2000) 3236.
[13] T. Kraska, U.K. Deiters, Int. J. Thermophys. 15 (1993) 261.
[14] K. Leonhard, T. Kraska, J. Supercritical Fluids 16 (1999) 1.
[15] Y. Tang, J. Chem. Phys. 109 (1998) 5935.
[16] F. Fornasiero, L. Lue, A. Bertucco, AIChE J. 45 (1999) 906.
[17] S.B. Kiselev, Fluid Phase Equilibria 147 (1998) 7.
[18] S.B. Kiselev, D.G. Friend, Fluid Phase Equilibria 162 (1999) 51.
[19] S.B. Kiselev, J.F. Ely, Ind. Eng. Chem. Res. 38 (1999) 4993.
[20] A. Jiang, J.M. Praustitz, J. Chem. Phys. 111 (1999) 5964.
[21] M.E. Fisher, Phys. Rev. 176 (1968) 257.
[22] R.B. Griffiths, J.C. Wheeler, Phys. Rev. A 2 (1970) 1047.
[23] W.F. Saam, Phys. Rev. A 2 (1970) 1461.
[24] M.A. Anisimov, A.V. Voronel, E.E. Gorodetskii, Sov. Phys. JETP 33 (1971) 605.
[25] S.B. Kiselev, High Temp. 26 (1988) 337.
[26] G.X. Jin, S. Tang, J.V. Sengers, Phys. Rev. E 47 (1993) 388.
[27] A.A. Povodyrev, G.X. Jin, S.B. Kiselev, J.V. Sengers, Int. J. Thermophys. 17 (1996) 909.
[28] M.Y. Belyakov, S.B. Kiselev, J.C. Rainwater, J. Chem. Phys. 107 (1997) 3085.
[29] S.B. Kiselev, Fluid Phase Equilibria 128 (1997) 1.
[30] S.B. Kiselev, J.C. Rainwater, Fluid Phase Equilibria 141 (1997) 129.
[31] S.B. Kiselev, J.C. Rainwater, M.L. Huber, Fluid Phase Equilibria 150/151 (1998) 469.
[32] S.B. Kiselev, J.C. Rainwater, J. Chem. Phys. 109 (1998) 643.
[33] S.B. Kiselev, M.L. Huber, Int. J. Refrig. 21 (1998) 64.
[34] H.S. Huang, M. Radosz, Ind. Eng. Chem. Res. 29 (1990) 2284.
[35] B.J. Alder, D.A. Young, M.A. Mark, J. Chem. Phys. 56 (1972) 3013.
[36] S.B. Kiselev, J.F. Ely, H. Adidharma, M. Radosz, Fluid Phase Equilibria, in press.
[37] S.B. Kiselev, D.G. Friend, Fluid Phase Equilibria 155 (1999) 33.
[38] M.Y. Belyakov, S.B. Kiselev, Physica A 190 (1992) 75.
[39] M.A. Anisimov, S.B. Kiselev, J.V. Sengers, S. Tang, Physica A 188 (1992) 487.
[40] A. Berestov, Sov. Phys. JETP 72 (1977) 338.
[41] M.E. Fisher, S.-Y. Zinn, P.J. Upton, Phys. Rev. B 59 (1999) 14533.
[42] P. Schofield, Phys. Rev. Lett. 22 (1969) 606.
[43] P. Schofield, J.D. Litster, J.T. Ho, Phys. Rev. Lett. 23 (1969) 1098.
[44] S.B. Kiselev, High Temp. 28 (1988) 42.
[45] S. Calero, M. Wendland, J. Fischer, Fluid Phase Equilibria 152 (1998) 1.
[46] M. Fermeglia, A. Bertucco, D. Patrizio, Chem. Eng. Sci. 52 (1997) 1517.
[47] H.S. Huang, M. Radosz, Ind. Eng. Chem. Res. 30 (1991) 1994.
[48] H.S. Huang, M. Radosz, Fluid Phase Equilibria 70 (1991) 33.
[49] Y. Takaishi, N. Kagawa, M. Uematsu, K. Watanabe, in: J.V. Sengers (Ed.), Proceedings of the 8th Symposium on Thermal Propulsion, Vol. 2, ASME, Gaithersburg, MD, 1982, pp. 387–395.
[50] J.W. Magee, W.M. Haynes, Int. J. Thermophys. 21 (2000) 113.

[51] M. Fukushima, K. Machidori, S. Kumano, S. Ohotoshi, in: Proceedings of the 14th Japan Symposium on Thermophysical Properties, Japan Society of Thermophysical Properties, Yokohama, Japan, 1993, pp. 275–278.
[52] E.W. Lemmon, A generalized model for the prediction of the thermodynamic properties of mixtures including vapor–liquid equilibrium, Ph.D. Thesis, University of Idaho, Moscow, ID, 1996.
[53] NIST Thermodynamic Properties of Refrigerant Mixtures Database, NIST REFPROP, v5.12, Natl. Inst. Stand. Technol., Gaitherburg, MD, 1987.
[54] Y. Higashi, in: Proceedings of the 19th International Congress on Refrigeration, Vol. IVa, International Institute of Refrigeration, The Hague, The Netherlands, 1995, pp. 297–305.
[55] Y. Higashi, T. Ikeda, Fluid Phase Equilibria 125 (1996) 139.
[56] L.F. Kells, S.R. Orfeo, W.H. Mears, Refrig. Eng. 63 (1955) 46.
[57] K. Watanabe, T. Tanaka, K. Oguchi, in: A. Cezarliyan (Ed.), Proceedings of the 7th ASME Thermal Propulsion Conference, ASME, Gaithersburg, MD, 1977, pp. 470–479.
[58] E. Fernandez-Fassnacht, F. Del Rio, Cryogenics 25 (1985) 204.
[59] M. Zander, in: J. Moszynski (Ed.), Proceedings of the 4th ASME Thermophysics Symposium, ASME, Gaithersburg, MD, 1968, pp. 114–123.
[60] L.M. Lagutina, Kholodilnaya Tekhnika (Russian) 43 (1966) 25.
[61] P.F. Malbrunot, P.A. Meunier, G.M. Scatena, W.H. Mears, K.P. Murphy, J.V. Sinka, J. Chem. Eng. Data 13 (1968) 16.
[62] J.W. Magee, Int. J. Thermophys. 17 (1996) 803.
[63] H.D. Baehr, R. Tillner-Roth, J. Chem. Thermodyn. 23 (1991) 1063.
[64] M. McLinden, private communication, Div. 838.08, NIST, Boulder, CO, 1980.
[65] R.C. McHarness, B.J. Eiseman, J.J. Martin, Refrig. Eng. 63 (1955) 31.
[66] M. Okada, M. Uematsu, K. Watanabe, J. Chem. Thermodyn. 18 (1986) 527.
[67] D.R. Defibaugh, G. Morrison, Fluid Phase Equilibria 80 (1992) 157.
[68] S. Kuwubara, H. Aoyama, H. Sato, K. Watanabe, J. Chem. Eng. Data 40 (1995) 112.
[69] G. Morrison, D.K. Ward, Fluid Phase Equilibria 62 (1991) 65.
[70] D.R. Defibaugh, G. Morrison, L.A. Weber, J. Chem. Eng. Data 39 (1994) 333.
[71] J.C. Holste, H.A. Duarte-Garza, M.A. Villamanan-Olfos, in: Proceedings of the 1993 ASME Winter Annual Meeting, Paper No. 93-WA/HT-60, ASME, New Orleans, 1993.
[72] H. Hou, J.C. Holste, B.E. Gammon, K.N. Marsh, Int. J. Refrig. 15 (1992) 365.
[73] Y. Higashi, Int. J. Thermophys. 16 (1995) 1175.
[74] M. Fukushima, Trans. Jpn. Assoc. Refrig. 7 (1990) 243.
[75] NIST Thermodynamic and Transport properties of Refrigerants and Refrigerant Mixtures, NIST REFPROP, V6.01, Natl. Inst. Stand. Technol., Gaitherburg, MD, 1998.
[76] E.W. Lemmon, R.T. Jacobsen, Int. J. Thermophys. 20 (1999) 1629.